

Energy-Level Structure of Ca^{41} from the $\text{Ca}^{40}(d,p)\text{Ca}^{41}$ Reaction*

T. A. BELOTE, A. SPERDUTO, AND W. W. BUECHNER

*Department of Physics and Laboratory for Nuclear Science, Massachusetts Institute of Technology,
Cambridge, Massachusetts*

(Received 8 December 1964)

The level structure of the nucleus Ca^{41} has been studied by the $\text{Ca}^{40}(d,p)\text{Ca}^{41}$ reaction at an incident deuteron energy of 7.00 MeV. Angular distributions have been measured for 120 levels below an excitation energy of 6.83 MeV, and those levels showing forward-stripping angular distributions have been analyzed using the distorted-wave Born approximation. Results on excitation energies, captured-neutron orbital angular momenta, and transition strengths are given for these levels. The data were further analyzed in terms of the shell model, and the unperturbed single-particle level positions with their corresponding spectroscopic factors were determined. For the $(1f_{7/2})$ single-particle level at $E_x=0.0$ MeV, $S=1.0$; $(2p_{3/2})$, $E_x=2.07$ MeV, $S=1.22$; $(2p_{1/2})$, $E_x=4.13$ MeV, $S=1.17$; $(1f_{5/2})$, $E_x=5.50$ MeV, $S=0.48$; $(1g_{9/2})$, $E_x \geq 4.98$ MeV, $S=0.07$; $(2d_{5/2})$, $E_x > 6.8$ MeV, $S=0.15$; and $(3s_{1/2})$, $E_x > 6.8$ MeV, $S=0.05$. The possible role of $(1d_{3/2})$ and $(2s_{1/2})$ shell-model hole states is also discussed.

I. INTRODUCTION

BECAUSE of the interest in nuclei in the $1f_{7/2}$ shell-model region, the previous work on the level structure of Ca^{41} carried out by Bockelman and Buechner¹ by means of the $\text{Ca}^{40}(d,p)\text{Ca}^{41}$ reaction has been extended to a region of higher excitation. Data on the angular distributions have also been extended to backward angles, and absolute cross sections have been measured for the transitions corresponding to levels in the energy region previously studied. The level structure of Ca^{41} and of other nuclei in this region have been discussed by French and Raz² and by Macfarlane and French.³ The energy-level structure of Ca^{41} should be especially simple from the standpoint of the shell model. Below about 7- or 8-MeV excitation, one expects the single-particle levels $(1f_{7/2})$, $(2p_{3/2})$, $(2p_{1/2})$, $(1g_{9/2})$, $(1f_{5/2})$, $(2d_{5/2})$, and $(3s_{1/2})$, corresponding to a single neutron's being in one of the possible shell-model orbitals outside of a ${}_{20}\text{Ca}^{40}$ core, represented by $(1s)$, $(1p)$, $(1d)$, and $(2s)$ closed shells. In this experiment, these single-particle levels should appear as proton groups showing stripping angular distributions and having large spectroscopic factors. Only the $(1f_{7/2})$ single-particle level was found to correspond to a single state in Ca^{41} ; the other single-particle levels showed various degrees of fragmentation.

Besides the states that were identified as members of single-particle levels, a large number of weak proton groups were also seen. The role of some of these weak groups that also have stripping angular distributions will be discussed in terms of stripping to hole states in Sec. IV G.

The analysis of the angular distributions was carried out using the distorted-wave Born approximation

(DWBA), and spectroscopic factors and l_n assignments were made from these calculations. The extension of the angular-distribution data to backward angles is important, since a J dependence on the shape of $l_n=1$ levels in the backward direction has been discovered by Lee and Schiffer.⁴ It is therefore possible to identify $J=\frac{1}{2}^-$ and $\frac{3}{2}^-$ states in the case of $l_n=1$ stripping.

A comparison has been recently given⁵ between the shell-model structure of Ca^{41} , as reported in this paper, and that of Ca^{49} , as reported by Kashy *et al.*⁶

II. EXPERIMENTAL PROCEDURE AND RESULTS

This experiment was carried out using the MIT broad-range, multiple-gap magnetic spectrograph.⁷ This allowed the simultaneous taking of data at 24 angles from 7.5 to 172.5 deg in the laboratory in 7.5-deg steps.

The target used in this experiment was thin Ca^{40} foil enriched to 99.99% in Ca^{40} . The Ca^{40} was obtained in the form of CaCO_3 from Oak Ridge National Laboratories and was evaporated in vacuum onto a few layers of Formvar using electron-gun bombardment.

The target was bombarded with a 7.00-MeV deuteron beam from the MIT-ONR Van de Graaff accelerator. Eastman Kodak 50 μ NTA nuclear-emulsion plates were used to detect the reaction protons, and the plates were scanned in 0.5 mm strips across the exposed zone. To cover the complete range of excitation from the ground state to 7 MeV, two exposures were necessary. One exposure was made with a magnetic field of 9228 G. This field setting causes the ground-state ($Q=6.146$ MeV) proton group to be near the top of the plates. The main exposure was carried out with a spectrograph field of 8509 G. This value of the field is such that the

⁴ L. L. Lee and J. P. Schiffer, Phys. Rev. Letters **12**, 108 (1964).

⁵ T. A. Belote, E. Kashy, A. Spurduto, H. A. Enge, and W. W. Buechner, Argonne National Laboratory Report No. ANL 6848, Atomic Energy Commission Report No. TTD 4500, Atomic Energy Commission Research and Development Report, 1964, edited by F. E. Throw (unpublished).

⁶ E. Kashy, A. Spurduto, H. A. Enge, and W. W. Buechner, Phys. Rev. **135**, B865 (1964).

⁷ H. A. Enge and W. W. Buechner, Rev. Sci. Instr. **34**, 155 (1963).

* This work has been supported in part through AEC Contract No. AT(30-1)-2098 with funds provided by the U. S. Atomic Energy Commission.

¹ C. K. Bockelman and W. W. Buechner, Phys. Rev. **107**, 1366 (1957).

² J. B. French and B. J. Raz, Phys. Rev. **104**, 1411 (1956).

³ M. H. Macfarlane and J. B. French, Rev. Mod. Phys. **32**, 567 (1960).

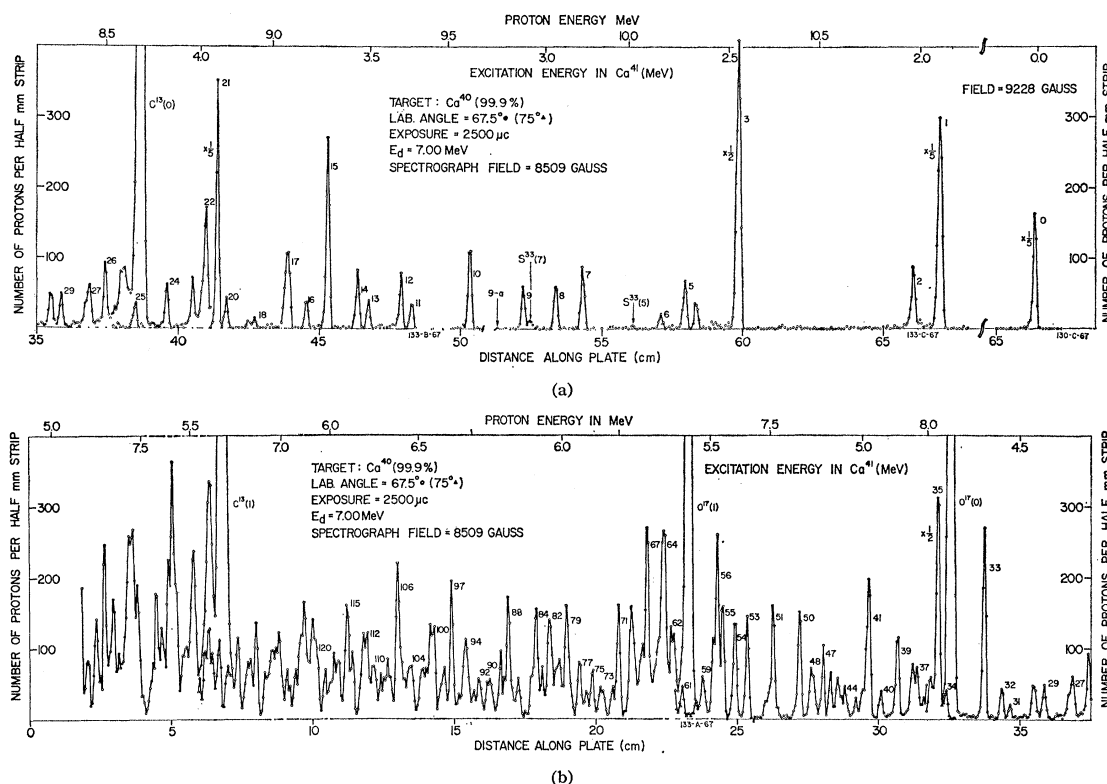


FIG. 1. (a) and (b). The measured proton spectra at $\theta_{\text{lab}} = 67.5^\circ$. The number of protons per 0.5 mm strip across the exposed zone is plotted versus plate distance in cm. The number to the right of each group is for identification of the states in Ca^{41} . Several contaminant groups are also identified.

first excited state ($E_x = 1.949$) is near the top of the plates. The main exposure was $2500 \mu\text{C}$; a shorter exposure of $500 \mu\text{C}$ was also made so that strong groups would be countable. Thin aluminum foils were placed over the plates in order to stop all particles except protons.

The proton spectrum observed at $\theta_{\text{lab}} = 67.5^\circ$ is shown in Figs. 1(a) and (b). The number to the right of each group is for identification; the numbering of the first twenty-five states is the same as that used by Braams⁸ and by Bockelman and Buechner.¹ One new very weak group, 9(a) at $E_x = 3.131$ MeV, was observed in the energy region below 4.2-MeV excitation.

The Q values and corresponding excitation energies of the states observed below 6.83-MeV excitation are given in Table I. For the states below 4.2-MeV excitation, the Q values given in Ref. 8 were adopted for this work. The Q values reported in Ref. 8 were recalculated using a $B\rho$ value of 331.750 kG cm for the polonium alpha-particle standard. This value of $B\rho$ corresponds approximately to a 0.1% increase over the Q values reported in Ref. 8. Q values for these transitions were also measured in this experiment and were found to agree to within ± 5 keV. Above 4.2-MeV excitation, the Q values given in Table I were calculated by

averaging the measured Q values over from three to ten angles at which the proton groups were best resolved. The errors in the Q values for the first 25 states are taken to be those given by Braams of from ± 4 to ± 7 keV. The errors for the Q values of states above 4.2 MeV are estimated to be $\leq \pm 10$ keV.

The target thickness was measured by elastic scattering of 3.00-MeV deuterons at angles between 45 and 90 deg, assuming Rutherford scattering. The elastic-scattering, angular-distribution data at this incident energy were found to deviate less than 6% from the assumed Rutherford shape for seven angles between 45 and 90 deg. The target used throughout this experiment was found to be $16.0 \mu\text{g}/\text{cm}^2$ in thickness. The measurement of absolute cross sections for the (d,p) reactions were therefore made possible. The error in the absolute cross section is estimated to be within $\pm 10\%$, with the ground-state (d,p) transition having a cross section at $\theta_{\text{max}} = 42^\circ$ of 4.8 ± 0.5 mb/sr.

The number of counts in each peak was summed, and, after transforming into center-of-mass cross section, was plotted versus center-of-mass angles. The angular distributions thus obtained are shown in Figs. 2 through 8. The errors arising from statistics and background subtraction are indicated in the figures by error flags on the data points.

⁸ C. M. Braams, Phys. Rev. **103**, 1310 (1956).

TABLE I. Results for the Ca⁴¹ level structure. LCO=lower cutoff.

Level No.	E_x (MeV)	Q (MeV)	θ_{\max} (deg)	l_n	$(d\sigma/d\Omega)\theta_{\max}$ mb/sr	$(2J+1)S$	
						LCO=3.4 F	LCO=0.0 F
0	0.000	6.146	40	3	4.80	8.00	5.90
1	1.949	4.197	19	1	25.0	3.76	3.30
2	2.017	4.129	28	2	0.82	0.78 ^a	
3	2.471	3.675	20	1	8.33	1.11	1.03
4	2.587	3.559	^b		0.14 ^b		
5	2.615	3.531			0.26		
6	2.680	3.466	<7.5	0	0.82 ^c	0.0352 ^c	0.027
7	2.893	3.253			0.19		
8	2.970	3.176			0.16		
9	3.059	3.087			0.13		
(9a)	3.131	3.015			0.03		
10	3.209	2.937			0.32		
11	3.378	2.768			0.07		
12	3.408	2.738	<7.5	0	0.84 ^c	0.0308	0.022
13	3.504	2.642			0.16		
14	3.536	2.610			0.20		
15	3.623	2.523	19	1	2.03	0.219	0.204
16	3.686	2.460			0.10		
17	3.740	2.406	24	2	1.1	0.283	0.216
18	3.841	2.305			0.03		
19	3.859	2.287	<7.5	0	0.28 ^c	0.0093	0.0078
20	3.925	2.221			0.06		
21	3.954	2.192	18	1	14.4	1.45	1.39
22	3.986	2.160			0.37		
23	4.027	2.119			0.12		
24	4.105	2.041			0.15		
25	4.198	1.948	16	1	0.18	0.0175	0.0154
26	4.295	1.851			0.16		
27	4.343	1.803			0.20		
28	4.357	1.789			0.12		
29	4.431	1.715			0.12		
30	4.462	1.684			0.12		
31	4.534	1.612			0.05		
32	4.561	1.585			0.08		
33	4.618	1.528	18	1	2.40	0.216	0.211
34	4.743	1.403			0.27		
35	4.765	1.381	18	1	4.72	0.414	0.410
36	4.788	1.358			0.22		
37	4.829	1.317	28	2	0.49	0.099	0.084
38	4.845	1.301			0.18		
39	4.894	1.252	44	3	0.53	0.69	0.61
40	4.944	1.202			0.07		
41	4.983	1.163	50	4	0.65	0.73	0.85
42	5.006	1.140			0.07		
43	5.024	1.122	<7.5	0	0.18 ^c	0.005	0.005
44	5.059	1.087	<7.5	0	0.25 ^c	0.0007	0.006
45	5.082	1.064	<7.5	0	0.48 ^c	0.014	0.012
46	5.107	1.039			0.41		
47	5.133	1.013			0.30		
48	5.162	0.984			0.28		
49	5.172	0.974			0.33		
50	5.208	0.938			0.625	0.119	0.101
51	5.297	0.849	31	2	0.13		
52	5.318	0.828			0.13		
53	5.381	0.765	16	1	0.675	0.0535	0.0535
54	5.421	0.725			0.48		
55	5.460	0.686	17	1	0.78	0.062	0.062
56	5.477	0.669	21	1	1.80	0.139	0.139
57	5.493	0.655	20	1	0.53	0.042	0.042
58	5.518	0.628			0.04		
59	5.527	0.619			0.18		
60	5.551	0.595			0.11		
61	5.597	0.549			0.08		
62	5.625	0.521			0.12		
63	5.635	0.511			0.12		
64	5.656	0.490	44	3	1.23	1.47	1.32
65	5.680	0.466	19	1	0.80	0.060	0.060
66	5.696	0.450			0.06		
67	5.714	0.432	17	1	1.75	0.133	0.133

^a See discussion, Sec. IV G. $(2J+1)S=0.78$, assuming a $(1d)$ orbital and 0.32 assuming a $(2d)$ orbital.

^b If no θ_{\max} is given, the cross sections at or near 30° are given. See Figs. 2 to 8.

^c For the case of $l_n=0$ transitions, the $\theta_{\text{lab}}=15^\circ$ cross sections are given. The values of $(2J+1)S$ are extracted by comparing the DWBA calculated cross sections to the experimental data at this angle.

TABLE I (continued)

Level No.	E_x (MeV)	Q (MeV)	θ_{\max} (deg)	l_n	$(d\sigma/d\Omega)\theta_{\max}$ mb/sr	$(2J+1)S$	
						LCO=3.4 F	LCO=0.0 F
68	5.730	0.416			0.41		
69	5.759	0.387			0.04		
70	5.764	0.382	30	2	1.05	0.182	0.156
71	5.813	0.333	44	3	0.56	0.65	0.60
72	5.832	0.314			0.20		
73	5.860	0.286			}0.17		
74	5.873	0.273					
75	5.901	0.245	20	1	0.82	0.061	0.061
76	5.920	0.226			0.09		
77	5.943	0.203			0.22		
78	5.977	0.169			0.12		
79	5.982	0.164			0.55		
80	6.011	0.135	<7.5	0	0.62 ^a	0.0198	0.018
81	6.026	0.120			0.4		
82	6.042	0.104			0.35		
83	6.070	0.076			0.16		
84	6.091	0.055			}0.53		
85	6.098	0.048					
86	6.149	-0.003			0.17		
87	6.176	-0.030			0.1		
88	6.188	-0.042	20	1	1.12	0.08	0.08
89	6.215	-0.069			0.14		
90	6.247	-0.101			}0.22		
91	6.262	-0.116					
92	6.284	-0.138			}0.26		
93	6.311	-0.165					
94	6.330	-0.184			}0.50		
95	6.338	-0.192					
96	6.366	-0.220			0.04		
97	6.385	-0.239	(17)	(1)	(1.04)	0.072	0.072
98	6.410	-0.264			}0.27		
99	6.423	-0.277					
100	6.453	-0.307			0.6		
101	6.468	-0.322			0.24		
102	6.473	-0.327			0.1		
103	6.488	-0.342			0.1		
104	6.525	-0.379			0.30		
105	6.555	-0.409			0.04		
106	6.568	-0.422	27	2	1.42	0.223	0.190
107	6.600	-0.454			}0.24		
108	6.612	-0.466					
109	6.638	-0.492			0.2		
110	6.655	-0.509			}0.3		
111	6.665	-0.519					
112	6.684	-0.538			}0.68		
113	6.699	-0.553					
114	6.738	-0.592			0.24		
115	6.755	-0.609			0.63		
116	6.787	-0.639			0.2		
117	6.800	-0.654			0.2		
118	6.810	-0.664			0.1		
119	6.835	-0.689			0.2		

The main contaminants observed in this experiment were the $C^{12}(d,p)C^{13}$ ground state ($Q=2.722$ MeV) and first excited state, and $O^{16}(d,p)O^{17}$ ground state ($Q=1.920$ MeV) and first excited-state transitions. Aside from the major contaminant peaks, weak peaks from contaminants of C^{13} , N^{14} , and S^{32} were also observed.

III. ANALYSIS

In order to determine the orbital angular momentum of the captured neutron and the transition strengths, the zero-range DWBA code JULIE (originated at Oak

Ridge National Laboratories by G. R. Satchler) was used to calculate the angular distributions for these reactions. The form of the potential used in the calculations was

$$U = -\frac{V}{e^x + 1} + 4iW' \frac{d}{dx'} \left(\frac{1}{e^{x'} + 1} \right) + V_c,$$

where

$$x = \frac{(r - r_0 A^{1/3})}{a}, \quad x' = \frac{(r - r_0' A^{1/3})}{a'},$$

and V_c is a Coulomb term representing the interaction

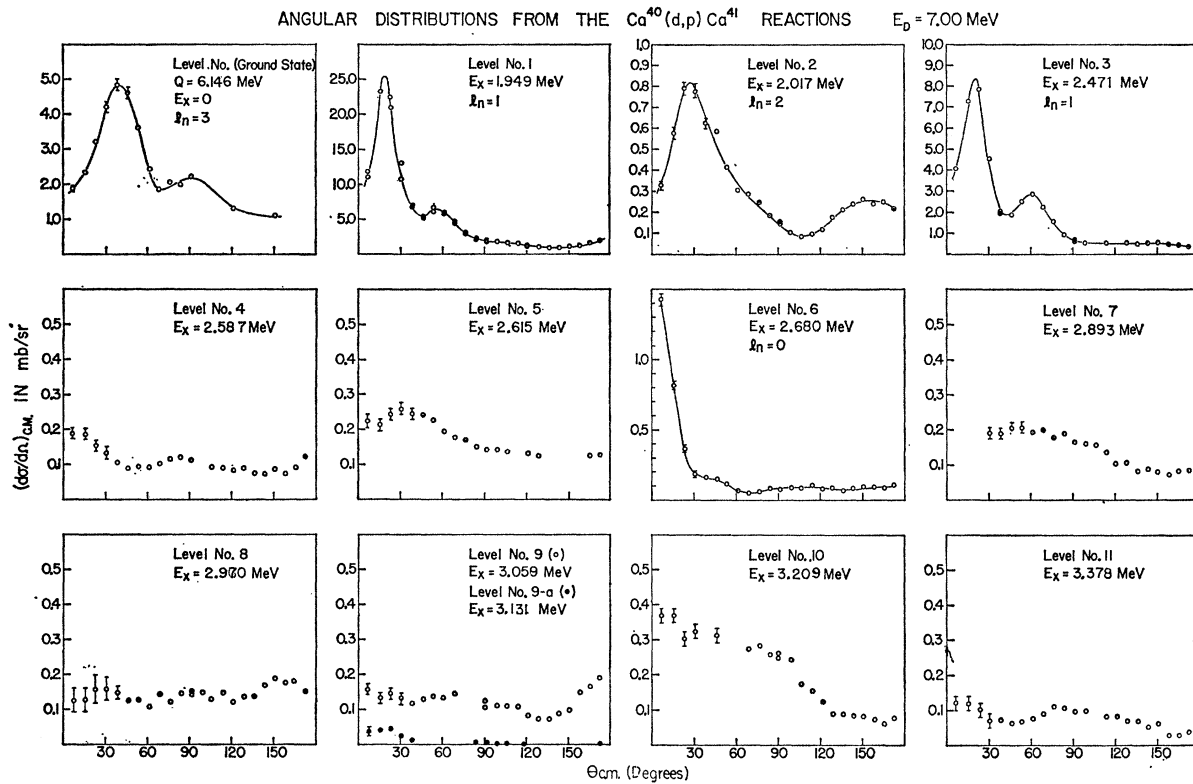


FIG. 2. Angular distributions of protons to the levels of Ca^{41} in mb/sr versus center-of-mass angle. Errors arising from statistics and background subtraction are indicated by error flags on the data points for data in the forward quadrant. The solid curves are drawn through the experimental data.

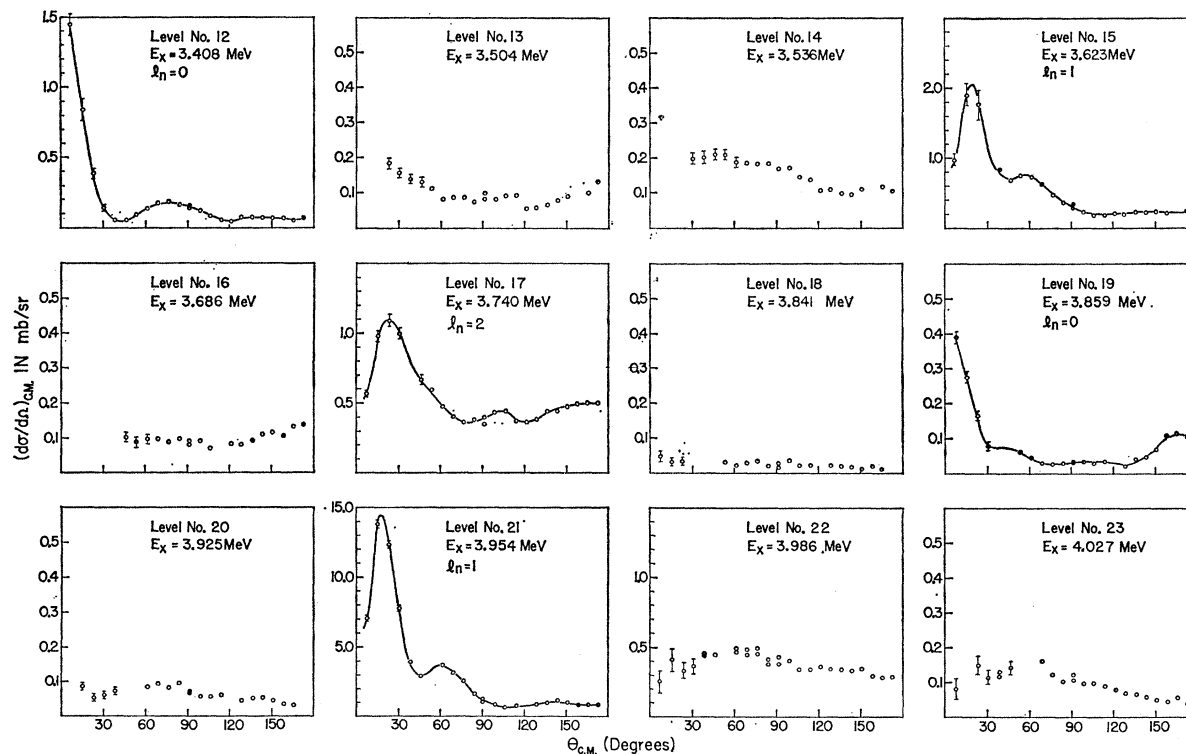


FIG. 3. Angular distributions of protons to the levels of Ca^{41} in mb/sr versus center-of-mass angle. Errors arising from statistics and background subtraction are indicated by error flags on the data points for data in the forward quadrant. The solid curves are drawn through the experimental data.

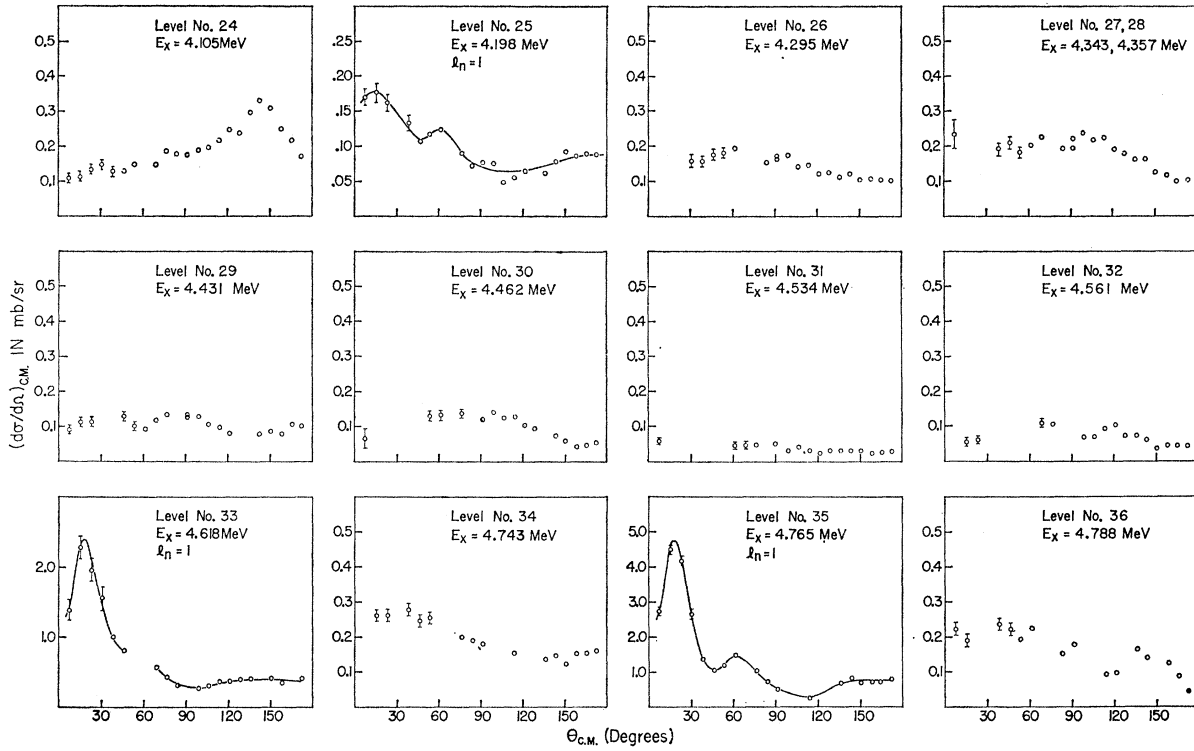


FIG. 4. Angular distributions of protons to the levels of Ca^{41} in mb/sr versus center-of-mass angle. Errors arising from statistics and background subtraction are indicated by error flags on the data points for data in the forward quadrant. The solid curves are drawn through the experimental data.

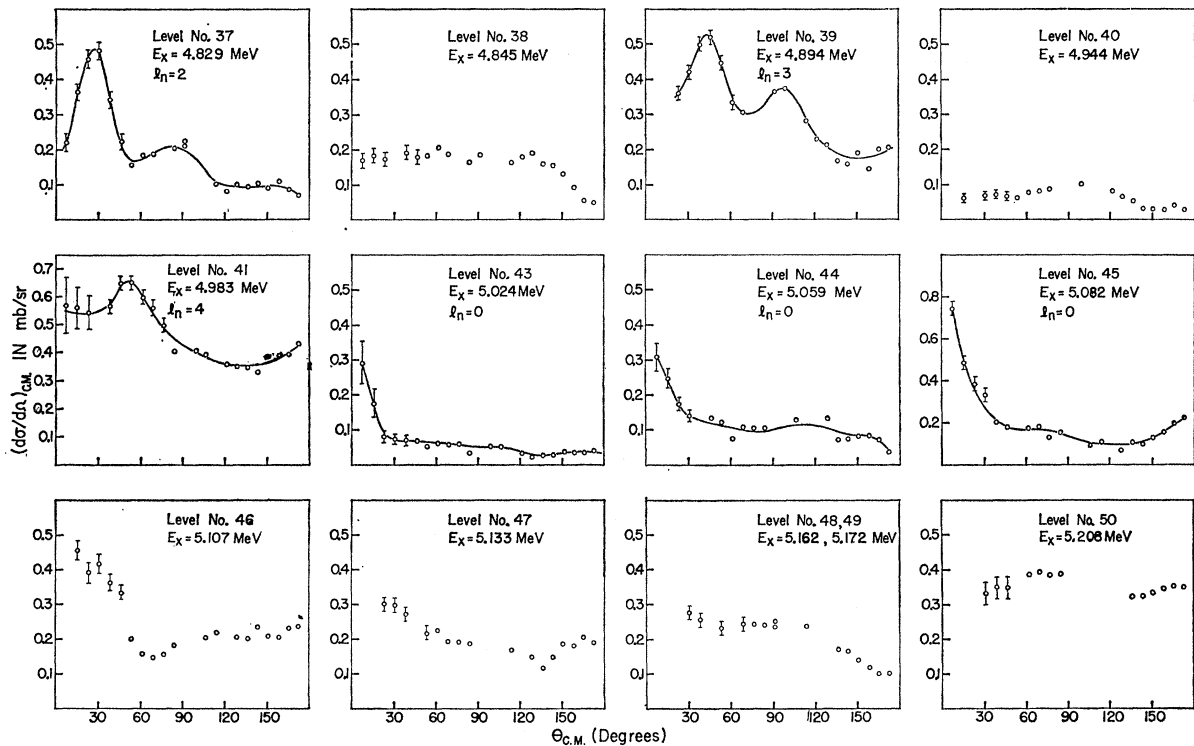


FIG. 5. Angular distributions of protons to the levels of Ca^{41} in mb/sr versus center-of-mass angle. Errors arising from statistics and background subtraction are indicated by error flags on the data points for data in the forward quadrant. The solid curves are drawn through the experimental data.

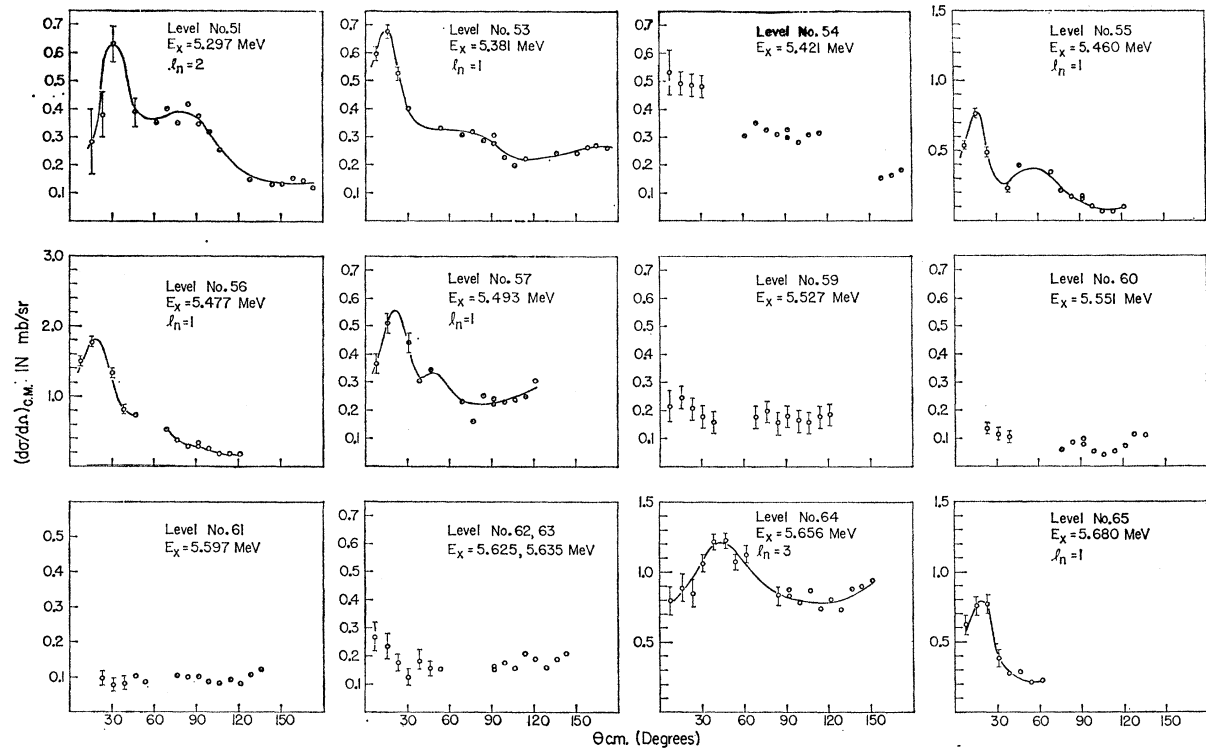


FIG. 6. Angular distributions of protons to the levels of Ca^{41} in mb/sr versus center-of-mass angle. Errors arising from statistics and background subtraction are indicated by error flags on the data points for data in the forward quadrant. The solid curves are drawn through the experimental data.

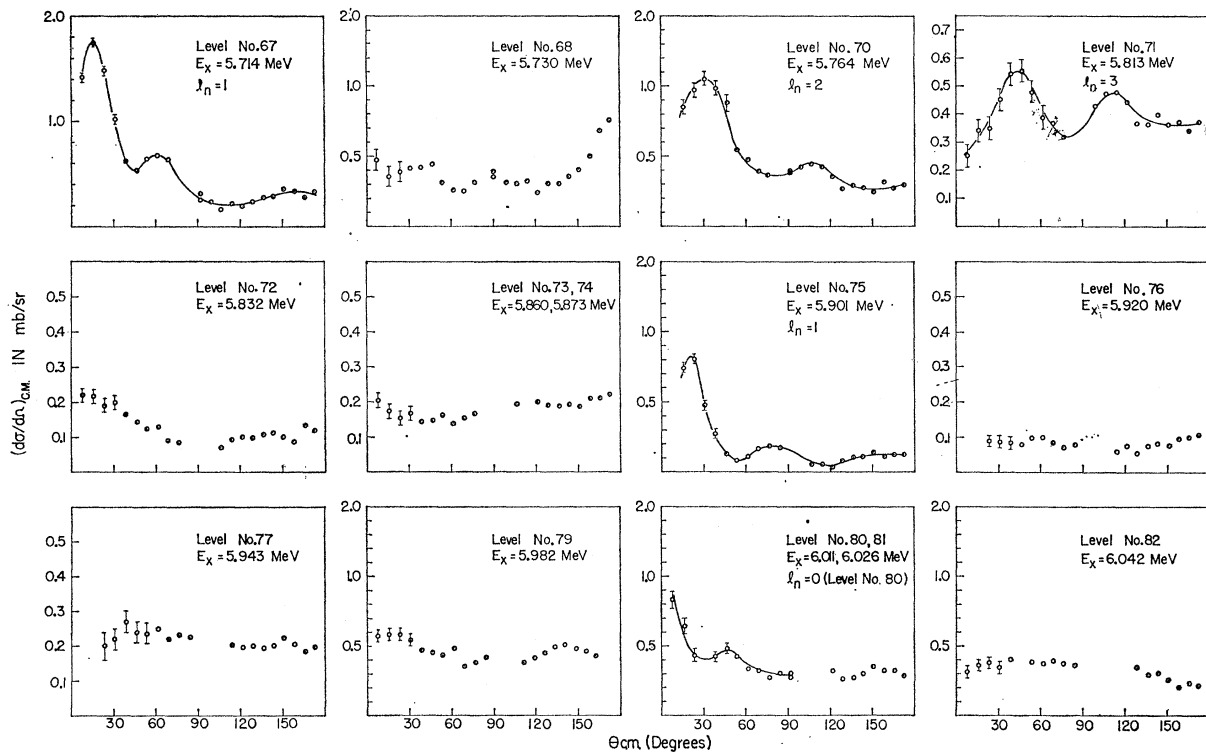


FIG. 7. Angular distributions of protons to the levels of Ca^{41} in mb/sr versus center-of-mass angle. Errors arising from statistics and background subtraction are indicated by error flags on the data points for data in the forward quadrant. The solid curves are drawn through the experimental data.

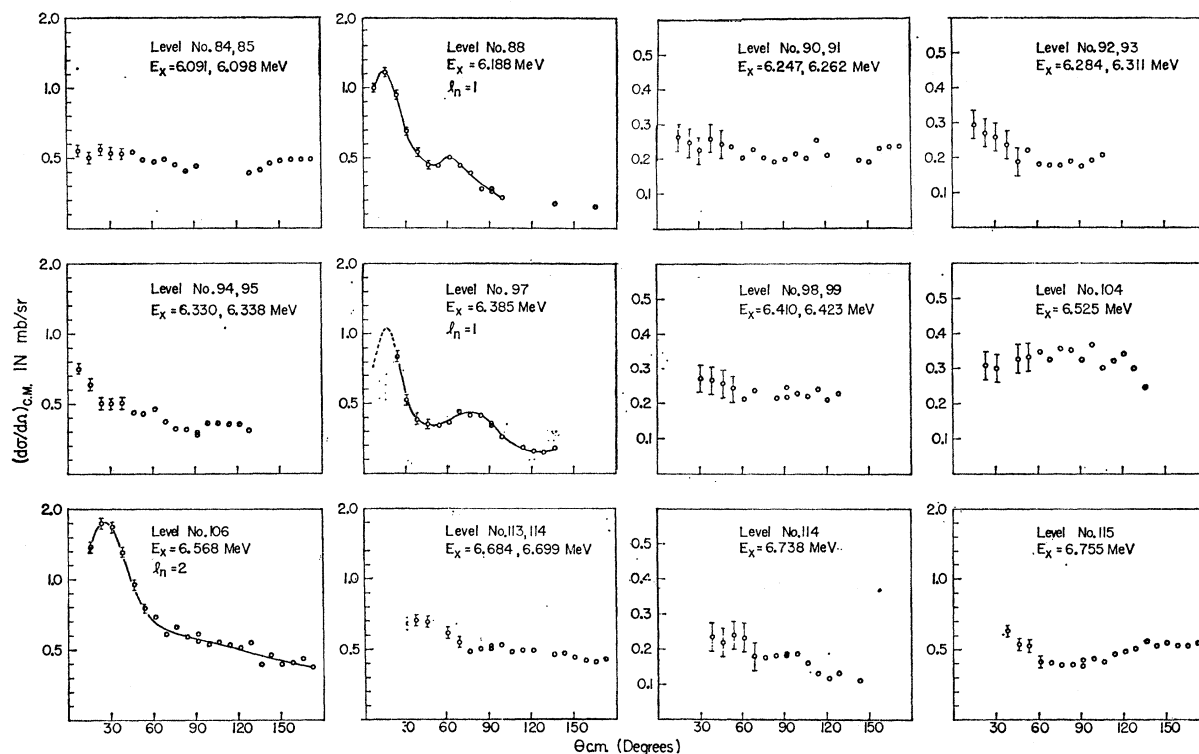


FIG. 8. Angular distributions of protons to the levels of Ca^{41} in mb/sr versus center-of-mass angle. Errors arising from statistics and background subtraction are indicated by error flags on the data points for data in the forward quadrant. The solid curves are drawn through the experimental data.

with a homogeneously charged sphere of radius $r_c = 1.3A^{1/3} \text{ F}$.⁹

The experimental cross sections are related to the DWBA results, $(d\sigma/d\Omega)_{\text{calc}}$, through the relation

$$(d\sigma/d\Omega) = \frac{3}{2} [(2J_f + 1)/(2J_i + 1)] (d\sigma/d\Omega)_{\text{calc}}. \quad (1)$$

The DWBA calculations were carried out for several values of the lower cutoff radius, and the l_n and $(2J+1)S$ values were extracted for each transition that showed a stripping pattern. The transition strengths were extracted using Eq. (1) at θ_{max} , except for the case of $l_n=0$ transitions where the 15-deg cross sections were used. The values of l_n and $(2J+1)S$ for each of the levels are given in Table I for a lower cutoff radius of 3.4 F and 0.0 F. The results are also presented graphically in Fig. 9. For the set of optical parameters used, a cutoff radius of 3.4 F seemed to give the most

reasonable set of results, and the spectroscopic factors and unperturbed single-particle level positions were calculated using this radius. A discussion of the validity of the DWBA has recently been given by Lee *et al.*¹⁰ who investigated the $\text{Ca}^{40}(d,p)\text{Ca}^{41}$ reactions leading to the ground, 1.949-, 2.471-, and 3.954-MeV levels at deuteron bombarding energies from 7 to 12 MeV.

Typical $l_n=0, 1, 2,$ and 3 calculated angular distributions, as compared with the experimental data, are shown in Fig. 10. For those levels not showing stripping, the values of their cross sections at 30 deg are given in Table I in order to indicate their relative intensities. In general, the levels not showing forward stripping were isotropic; however, some of these angular distributions had variations in their differential cross sections of a factor of 2 or more.

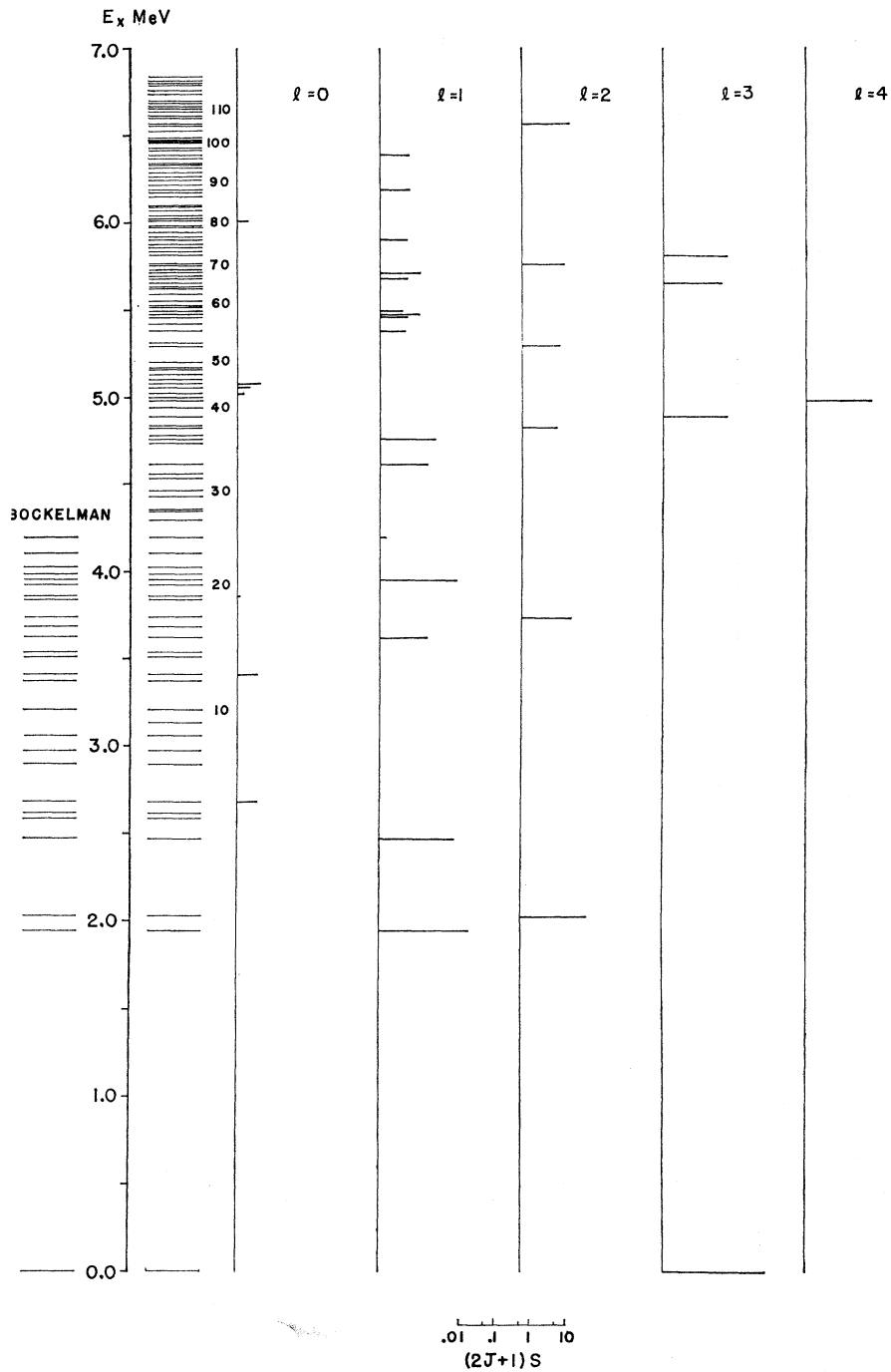
IV. SHELL-MODEL ASSIGNMENTS

On the basis of the simple shell model, one expects to find only a few strong transitions leaving the neutron in an allowed shell-model orbital, whereas experimentally many transitions are seen. In this section, assignments to some of the transitions are made using the shell model as a guide in grouping them into their single-particle components.

⁹ See R. H. Bassel, R. M. Drisko, and G. R. Satchler, Oak Ridge National Laboratory Report No. 3240, (Office of Technical Services, Washington 25, D. C. 1963) for further definition of the symbols used in this equation. The parameters used for the analysis of these data were obtained from an analysis of 7.0-MeV elastic-scattering data of deuterons from Ca^{40} carried out by G. R. Satchler. The parameters were

	V (MeV)	r_0 (F)	a (F)	W' (MeV)	r_0' (F)	a' (F)
For (d)	162	0.703	1.079	10.3	1.712	0.602
For (p)	50.2	1.25	0.65	10.3	1.25	0.47
For (n)		1.25	0.65			

¹⁰ L. L. Lee, J. P. Schiffer, B. Zeidman, G. R. Satchler, R. M. Drisko, and R. H. Bassel, Phys. Rev. **136**, B971 (1964).



Energy Levels of Ca^{41}

FIG. 9. Energy-level diagram of Ca^{41} , with strengths $(2J+1)S$ shown for the $l_n=0, 1, 2, 3,$ and 4 transitions.

A. The $(1f_{7/2})$ Ground State

A strong $l_n=3$ transition is observed to the ground state. No other $l_n=3$ level was observed below 4.8-MeV excitation, and an assignment of $J^\pi = \frac{7}{2}^-$ is given to this state. This is in agreement with the earlier work of

Ref. 1. The spectroscopic factor for this transition should be near to 1.0. Macfarlane and French³ have pointed out that ground-state wave functions involving as much as 40% $(1d_{3/2})^{-2}$ admixtures for Ca^{40} and Ca^{41} would reduce the spectroscopic factor only

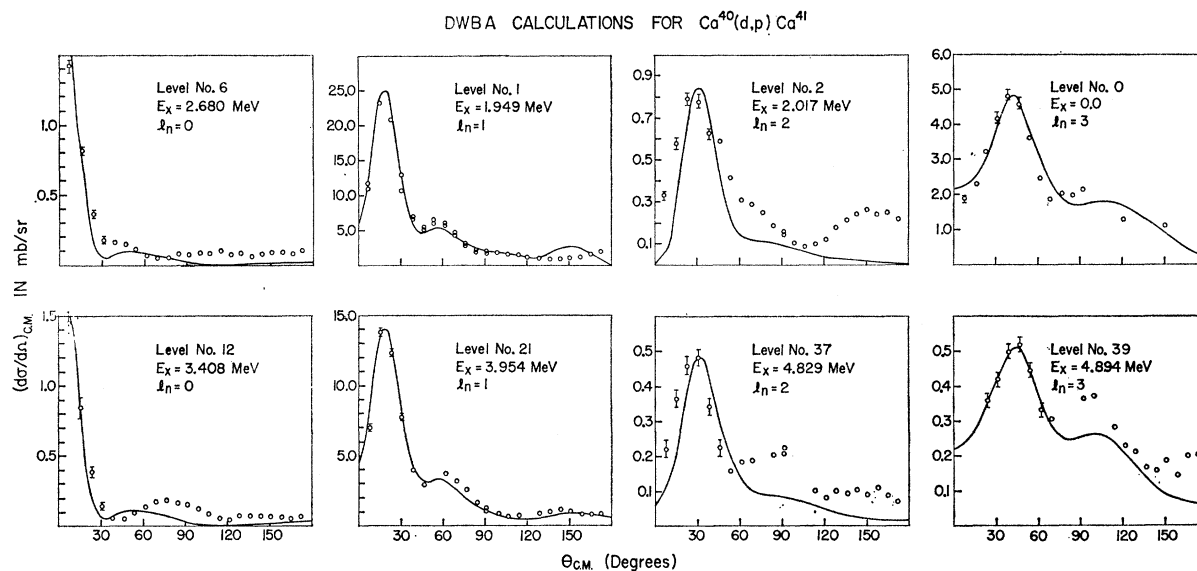


Fig. 10. Typical $l_n=0, 1, 2$, and 3 DWBA angular distributions compared with the experimental data. The curves have been matched at the maximum cross section (15° for the case of $l_n=0$) to yield the strengths given in Table I.

10% for this transition. As discussed in Sec. III, a lower cutoff radius of $3.4 F$ gives $S=1.0$ for this level.

B. The $(2p_{3/2})$ Single-Particle Level

Near 2.0-MeV excitation, two strong $l_n=1$ transitions were observed: $E_x=1.949$ and 2.471 MeV. An assignment of $J^\pi=\frac{3}{2}^-$ has been given to these levels by Trumphy¹¹ and by Lee *et al.*¹² The angular distributions of these two levels, together with four of the five $l_n=1$ levels assigned as $J^\pi=\frac{1}{2}^-$, are shown in Fig. 11. The angular distributions of the two levels assigned $J^\pi=\frac{3}{2}^-$ are relatively flat near $\theta=100^\circ$, whereas the $J^\pi=\frac{1}{2}^-$ levels show a dip at this angle. Using these assignments, S was calculated for each transition, and the unperturbed single-particle energy for the $(2p_{3/2})$ level was calculated by weighting the excitation energies by S . The unperturbed energy thus obtained for the $(2p_{3/2})$ single-particle level is 2.07 MeV, with a sum of spectroscopic factors equal to 1.22 for the two $J^\pi=\frac{3}{2}^-$ levels. These values, along with those for the other single-particle levels, are summarized in Table II.

C. The $(2p_{1/2})$ Single-Particle Level

Five $l_n=1$ levels, $E_x=3.623, 3.954, 4.198, 4.618,$ and 4.765 , were observed in the region about 4.0-MeV excitation. As was pointed out in the preceding section, an assignment of $J^\pi=\frac{1}{2}^-$ was given to these levels on the basis of the dip in their angular distributions near 100° . The $3.623-$, $3.954-$, $4.618-$, and 4.765 -MeV levels are shown in Fig. 10; the weak 4.198 -MeV level

is shown in Fig. 2. An assignment of $\frac{1}{2}^-$ to the 3.954 -MeV level is consistent with that of Bockelman and Buechner¹ and that of Lee *et al.*^{4,12} The values of the spectroscopic factors for each of these five transitions are given in Table II. The unperturbed single-particle energy calculated from these five levels is 4.13 MeV with a sum of spectroscopic factors of 1.17 . The fragmenta-

TABLE II. Shell-model level structure of Ca⁴¹.

Level No.	E_x (MeV)	Shell-model configuration	S	Un-perturbed No. of levels	level position	ΣS
0	0.000	$(1f_{7/2})$	1.00	1	0.00	1.0
1	1.949	$(2p_{3/2})$	0.94	2	2.07	1.22
3	2.471		0.28			
15	3.623	$(2p_{1/2})$	0.11	5	4.13	1.17
21	3.954		0.73			
25	4.198		0.01			
33	4.618		0.11			
35	4.765		0.21			
39	4.894	$(1f_{5/2})$	0.12	3	5.50	0.48
64	5.656		0.25			
71	5.813		0.11			
41	4.983	$(1g_{9/2})$	0.07	1	≥ 4.98	0.07
6	2.680	$(3s_{1/2})$	0.018	7	> 6.8	0.06
12	3.408		0.015			
19	3.859		0.005			
43	5.024		0.002			
44	5.059		0.003			
45	5.082		0.007			
80	6.011		0.010			
17	3.740	$(2d_{5/2})$	0.047	5	> 6.8	0.151
37	4.829		0.017			
51	5.297		0.020			
70	5.764		0.030			
106	6.568		0.037			
2	2.017	$[(1f_{7/2})^2(1d_{3/2})^{-1}]$	0.19

¹¹ G. Trumphy, Nucl. Phys. 2, 664 (1957).

¹² L. L. Lee, J. P. Schiffer, and D. S. Gemell, Phys. Rev. Letters 10, 496 (1963).

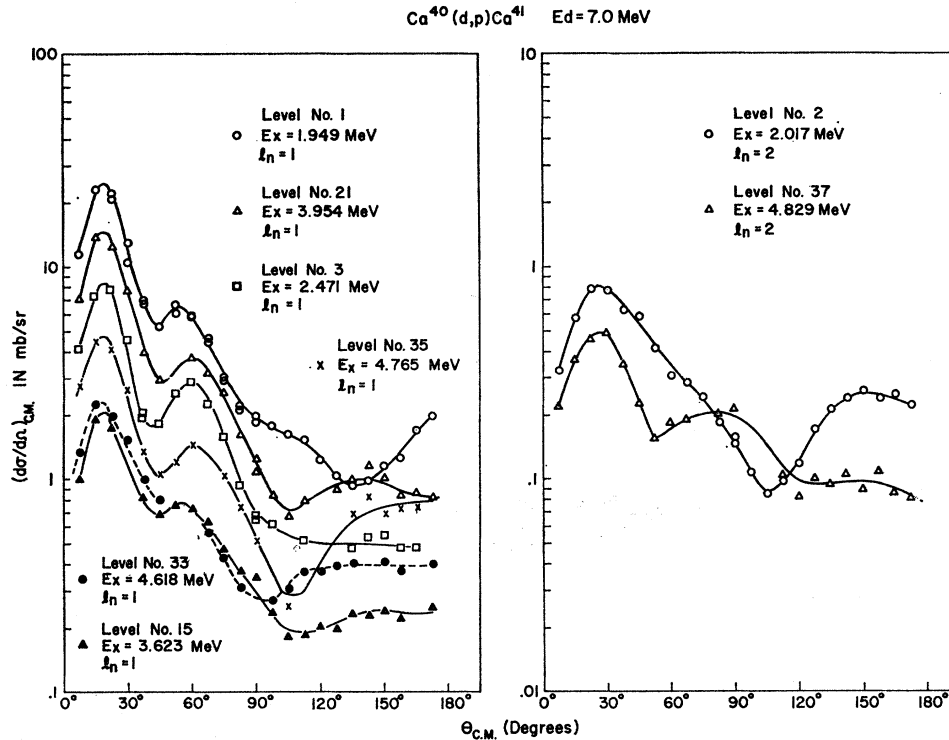


FIG. 11. Typical $l_n=1$, $(2p_{3/2})$ and $(2p_{1/2})$, angular distributions. The 1.949- and 2.471-MeV $(2p_{3/2})$ levels show a flat region near 100 deg, whereas the 3.623-, 3.954-, 4.618-, and 4.765-MeV $(2p_{1/2})$ levels show dips near 100°. Angular distributions of two $l_n=2$ levels, $E_x=2.017$ and 4.829 MeV, are shown to illustrate the difference in shape. See text for discussion.

tion of the $(2p_{1/2})$ single-particle level over 1.1 MeV of excitation is about one-third the unperturbed $(2p_{1/2})$ excitation energy. The splitting between the $(2p_{3/2})$ and $(2p_{1/2})$ unperturbed single-particle positions is 2.06 MeV, as compared with the 2.03-MeV splitting in Ca^{40} observed by Kashy *et al.*⁶ and the 1.83-MeV splitting in Ar^{41} observed by Kashy, Hoogenboom, and Buechner.¹³

D. The $(1f_{5/2})$ Single-Particle Level

Using the value of 2.06 MeV for the splitting between the $(2p_{3/2})$ and $(2p_{1/2})$ single-particle levels and assuming the splitting to be proportional to $(2l+1)$, it was found that the $(1f_{5/2})$ level should be near 4.9-MeV excitation. In this region of excitation, three $l_n=3$ levels, $E_x=4.894$, 5.656, and 5.813 MeV, were observed and were assumed to be fragments of the $(1f_{5/2})$ single-particle level. The values of the spectroscopic factors for these transitions are given in Table II, assuming $J^\pi = \frac{5}{2}^-$. The unperturbed single-particle energy of these levels is 5.50 MeV, with a sum of spectroscopic factors equal to 0.47. Since in this region of excitation weak $l_n=3$ transitions are difficult to observe, it is probable that some weak $1f_{5/2}$ levels were missed.

¹³ E. Kashy, A. M. Hoogenboom, and W. W. Buechner, *Phys. Rev.* 124, 1917 (1961).

E. The $(1g_{9/2})$ Single-Particle Level

One $l_n=4$ level was observed in this experiment at 4.983-MeV excitation, having a spectroscopic factor of 0.07 assuming $J^\pi = \frac{9}{2}^+$. Because of the difficulty in observing $l_n=4$ transitions, some $l_n=4$ transitions were probably missed in this experiment.

F. The $(2d_{5/2})$ and $(3s_{1/2})$ Single-Particle Levels

A total of six $l_n=2$ and seven $l_n=0$ levels were seen below 6.8-MeV excitation, and their energies and spectroscopic factors are tabulated in Table II. The sum of spectroscopic factors for all $l_n=2$ levels below 6.8 MeV, except for the 2.017-MeV level which is discussed in Sec. G, is 0.15, and for all $l_n=0$ levels, also below 6.8 MeV, it is 0.05. This indicates that both the $(2d_{5/2})$ and $(3s_{1/2})$ single-particle levels lie above 6.8 MeV in Ca^{41} . This result is consistent with that of Kashy *et al.*⁶ on the levels of Ca^{40} .

G. Stripping to Hole States

In the preceding sections, stripping reactions that leave the neutron in higher shell-model orbitals have been discussed. It is also possible that the stripping reactions take place by lower shell-model orbitals, for example, $(1d_{3/2})$ and $(2s_{1/2})$. This would be the case if the ground-state wave function of Ca^{40} were not described

simply as a double closed-shell configuration but instead also had components such as $[(1d_{3/2})^{-2}(1f_{7/2})^2]$ and $[(2s_{1/2})^{-2}(1f_{7/2})^2]$. Evidence for a $(1d_{3/2})^{-2}$ component in the Ti⁴⁶ ground-state wave function has been pointed out by Kashy and Conlon¹⁴ with the Ti⁴⁶(*p,d*)Ti⁴⁵ reaction, in conjunction with the work of Rapaport¹⁵ on the Ti⁴⁶(*d,p*)Ti⁴⁷ reaction. It is suggested that such may also be the case for the $l_n=2$ level at $E_x=2.017$ MeV. Such a possibility has been previously discussed by Macfarlane.³ Also, it is interesting to note, in view of the results of Lee and Schiffer,⁴ that the angular distribution of this $l_n=2$ transition differs considerably from other $l_n=2$ angular distributions for angles greater than 60 deg. Figure 11 shows this level compared with the $l_n=2$ level at 4.829-MeV excitation. Assuming $J^\pi=\frac{3}{2}^+$ and stripping to a $1d_{3/2}$ hole, it was found that the 2.017-MeV transition has a spectroscopic value of 0.19. This value is consistent with an admixture of about 40% $[(1d_{3/2})^{-2}(1f_{7/2})^2]$ configuration in the Ca⁴⁰ ground-state wave function. A similar explanation may hold for some of the other levels, in particular the low-lying $l_n=0$ levels at 2.677- and 3.405-MeV excitation, which may indicate admixtures of $[(2s_{1/2})^{-2}(1f_{7/2})^2]$ configurations in the Ca⁴⁰ ground state.

V. CONCLUSION

The level structure of Ca⁴¹ appears more complicated than one expects on the basis of the simple shell model.

¹⁴ E. Kashy and T. W. Conlon, Phys. Rev. **135**, B389 (1964).

¹⁵ J. Rapaport, Ph.D. thesis, M.I.T. 1963 (unpublished).

The role of residual interactions is indicated by the fragmentation of the single-particle levels into several components. Also, the low-lying $l_n=2$ and $l_n=0$ transitions, which have been interpreted as stripping-to-hole states, indicate a more complicated configuration for the Ca⁴⁰ ground state than a simple double closed-shell configuration. Aside from the levels that show stripping, there are approximately ninety other levels up to 6.8-MeV excitation which do not show stripping and for which no assignments have been made. This situation should be contrasted with the somewhat simpler case of Ca⁴⁹ discussed in Ref. 6 where only ten excited states below 6.2-MeV excitation were observed. Nevertheless, most of the strong levels showing stripping angular distributions are consistent with a shell-model interpretation for the structure of Ca⁴¹.

ACKNOWLEDGMENTS

The authors would like to thank the MIT scanning group and, in particular, W. A. Tripp and Mrs. Mary Fotis for the careful scanning of the nuclear-track plates. We should like to thank Dr. G. R. Satchler for making available to us the optical-model parameters used in the analysis and Hsueh-yi Chen for carrying out the DWBA calculations. The authors are especially indebted to Dr. J. Rapaport for his help in the earlier part of this work. Finally, we wish to acknowledge the discussions with Dr. E. Kashy on comparisons with his recent work on the Ca⁴⁹ level structure. The manuscript was prepared by Mrs. Mary E. White.